

Optimality of linear vacancy defect for skyrmion nucleation

Maria N. Potkina^{1,a}, Igor S. Lobanov^{1,b}¹ITMO University, 197101 St. Petersburg, Russia^apotkina.maria@yandex.ru, ^blobanov.igor@gmail.com

Corresponding author: M. N. Potkina, potkina.maria@yandex.ru

PACS 82.20.Pm, 34.10.+x, 75.40.Mg

ABSTRACT Magnetic skyrmions offer a pathway to ultra-dense, low-power memory, but writing them efficiently remains a challenge. Using atomistic spin simulations and minimum energy path calculations in a PdFe/Ir(111) film, we show that deliberately placing linear chains of four atomic vacancies cuts the skyrmion nucleation barrier nearly in half-down to 44.7 meV at 3.75 T-compared to 85 meV in a pristine track. Linear defects excel because they remove high-energy core regions during skyrmion creation while minimally disturbing its outer negative energy halo during depinning. This geometry-driven effect relies only on generic energy density profiles, making it broadly applicable to all skyrmion-hosting materials.

KEYWORDS transition state theory, topological magnetic solitons, nucleation, racetrack memory.

ACKNOWLEDGEMENTS The study was supported by the Russian Science Foundation grant No. 24-72-00089, <https://rscf.ru/en/project/24-72-00089/>.

FOR CITATION Potkina M.N., Lobanov I.S. Optimality of linear vacancy defect for skyrmion nucleation. *Nanosystems: Phys. Chem. Math.*, 2025, **16** (3), 317–324.

1. Introduction

Magnetic skyrmions (Sks) are topological spin structures that arise in chiral magnetic materials [1,2]. Their nanometer-scale size, high mobility, and the low current densities required for their manipulation make them promising candidates for information carriers in future storage devices [3]. The intentional creation, destruction, and control of Sk are essential challenges that must be addressed to facilitate their application in future spintronic technologies.

One of the factors that influences the control of Sks is their interaction with impurities that are inevitably present in the sample. Impurity-induced pinning has been shown to affect Sk mobility [4], potentially leading to slower operation of spintronic devices. Furthermore, pinned Sks exhibit lower stability compared to free Sks [5–8], which may lead to a shorter information storage lifespan.

Impurities can also serve a beneficial role in skyrmionic applications. For instance, impurities can be utilized to create repelling and attracting rails for Sks guides [8–10]. Boundary notches can be employed to position Sks by creating potential wells [11–13]. Experimental evidence shows that Sks nucleate more readily on impurities [14], suggesting that artificially created impurities can act as effective nucleation centers for Sks. Additionally, the destructive effects of defects on Sks have been proposed for use in the development of Sk deletion devices [15].

Effective use of Sks requires a thorough understanding of their interactions with defects of various types, sizes, and geometries. Numerous studies have focused on the theoretical studies using various approaches, including atomistic models [7–9, 16–18], micromagnetic models through the solution of the Landau-Lifshitz-Gilbert equation [19–26], rigid models described by the Thiele equation [25–27], as well as analytical approaches [28–30].

However, Sk nucleation on impurities remains insufficiently explored. This paper will focus on investigating the influence of the geometry and size of atomic-scale non-magnetic defects on the processes of Sk creation and depinning. By calculating the activation barriers for Sk creation and depinning, we aim to determine the optimal defect type for efficient Sk nucleation in future memory and computing devices.

2. Method and simulated system

A thin magnetic film is modelled within the generalized Heisenberg model, which is a standard tool for Sk simulation with atomistic resolution. Symmetric (Heisenberg) exchange, Dzyaloshinskii-Moriya interaction (DMI), anisotropy, and the Zeeman energy of interaction with an external field \mathbf{B} contribute to the total energy E :

$$E = -J \sum_{\langle i,j \rangle} \mathbf{S}_i \cdot \mathbf{S}_j - \sum_{\langle i,j \rangle} \mathbf{D}_{ij} \cdot (\mathbf{S}_i \times \mathbf{S}_j) - \mu \sum_i \mathbf{B} \cdot \mathbf{S}_i - K \sum_i S_{i,z}^2. \quad (1)$$

The summation is taken over all pairs $\langle i, j \rangle$ of nearest neighbours atoms, and over all atoms i of the crystal lattice, except for non-magnetic impurities (vacancies). Here J is the symmetric exchange parameter; \mathbf{D}_{ij} is the DMI vector, which

lies in the film plane and is perpendicular to the vector connecting atomic sites i and j , thus stabilizes Néel-type Sk. $K > 0$ is the anisotropy constant corresponding to an easy axis along the coordinate axis z perpendicular to the film; \mathbf{B} is the external magnetic field, applied parallel to z -axis; and \mathbf{S}_i is a three-dimensional unit vector in the direction of the magnetic moment at the site i . The magnitude of the magnetic moment, μ , is assumed to be the same at all sites. Impurities are treated as vacancies without magnetic moments in the lattice. The system parameters correspond to experimentally observed Sk in a Pd/Fe bilayer on an Ir(111) substrate: a triangular crystal lattice, $\mu B = 0.093J$, $K = 0.07J$, $D = |\mathbf{D}_{ij}| = 0.32J$, and $J = 7$ meV [31]. The parameters correspond to an isolated free Sk with a radius of approximate $4a = 1.08$ nm, where $a = 0.27$ nm is the lattice constant. We apply periodic boundary conditions along the x -axis and assume free boundaries along the y -axis, thereby simulating a track of finite width. Track length $l_x = 60a$ and width $l_y = 60a \sin \frac{\pi}{3}$ are the same for all simulations and are large enough to prevent Sk self interaction and interaction with the track boundaries. Nonmagnetic impurity cluster (IC) is simulated by removing a cluster of the spins and excluding corresponding terms from energy (1).

(Meta)stable states correspond to local minima on the multidimensional energy surface defined by equation (1) for E , as a function of the directions of all magnetic moments \mathbf{S} . For the given set of parameters, the ground state corresponds to the ferromagnetic (FM) state, with a perturbation near the IC and rotating moments at the free boundary. A Sk pinned (attached) to the IC and a free Sk form two distinct metastable states. Metastable states were computed using a constrained nonlinear conjugate gradient method adapted for magnetic systems [32]. Activation barriers for the transition between pinned, depinned Sk and FM phase were computed using minimum energy path (MEP), which provides the most probable transition scenario [33]. The energy maximum along the MEP determines the first-order saddle point on the energy surface (transition state). Activation barrier is computed as difference between energies of the transition state and the initial one. MEP is approximated by its discretization defined by several states of magnetization vectors (called images) computed numerically. In our computations we used 15 to 50 images along each path and employed the string method for the numerical optimization of the MEP [34, 35]. For all paths, the initial state was FM and final state corresponds to the relaxed isolated Sk, completely separated from the IC.

3. Results

We investigated the processes of Sk nucleation on multiatomic nonmagnetic impurities, taking into account their geometry and size. To this end, we calculated MEP between two states: the initial state represented a FM configuration with the IC, while the final state corresponded to a Sk that was separated from the IC. We considered three types of IC shapes: compact, angular, and linear. A compact IC is defined as a cluster of atoms arranged in such a way that it has the smallest boundary for a given number of atoms. Examples of compact ICs are shown in the upper row of the right panel in Fig. 1. A linear IC refers to a cluster of atoms aligned along a lattice vector, thus maximizing the boundary; examples are shown in the lower row of Fig. 1. An angular IC consists of two linear ICs oriented along different lattice vectors that originate from a single lattice site. We denote the number of atoms forming the IC as N . The resulting nucleation barriers for the three types of ICs as a function of N are presented in the left panel of Fig. 1.

For $N = 1$ and 2, the ICs of different types are identical; however, starting from $N \geq 3$, the ICs differ in geometry, which, as shown in the plot, leads to variations in the corresponding nucleation barriers. For all values of N , linear ICs yield the lowest barrier for Sk nucleation. It is also evident that, for all types of ICs, there exists an optimal impurity size at which the barrier is minimized. The reasons for these two observations are discussed below.

Effect of Linear IC Size on the Nucleation Barrier. The mechanism of Sk nucleation on a linear IC is illustrated in the lower panel of Fig. 2. As the domain wall winds around the IC, it begins to expand until a Sk core is formed. The Sk then shifts toward one end of the IC and subsequently detaches from it. It is worth noting that for long ICs, Sk creation occurs on one side of the impurity, while the magnetization texture on the other side remains unaffected, until very late stages of the creation process.

The upper panel of Fig. 2 presents the MEPs for several values of N . Each path exhibits an intermediate minimum corresponding to a Sk pinned to the IC. Thus, the nucleation process can be divided into two stages. The first stage involves the creation of a Sk on the IC, where the initial state is a homogeneous FM configuration with an IC, and the final state is a Sk localized at the IC (insets 1-2-3 in Fig. 2). The second stage is the depinning of the Sk from the IC, where the initial state is a Sk localized at the IC and the final state is a free Sk (insets 3-4-5 in Fig. 2). For clarity, we will refer to the first stage as *creation*, while encompassing both stages-including depinning from the IC-as *nucleation*.

The nucleation barrier is defined by the maximum energy along the MEP, with the energy of the FM state set to zero. As illustrated in Fig. 2, the energy of the transition state for creation rapidly decreases with increasing N , while the energy for depinning increases moderately. Energy of intermediate metastable state (the pinned Sk) also decreases with increase of N , but more slowly. For large N , the energy of the pinned Sk approaches the energy of the transition state for the creation process.

The obtained dependencies of the energy maxima for both stages, within the range of N up to 15, are presented in Fig. 3a. For small IC sizes up to $N = 4$, the barrier for creation dominates. However, as the size increases, depinning starts to take precedence. The maximum along the entire path determines the barrier for Sk nucleation at a specific N

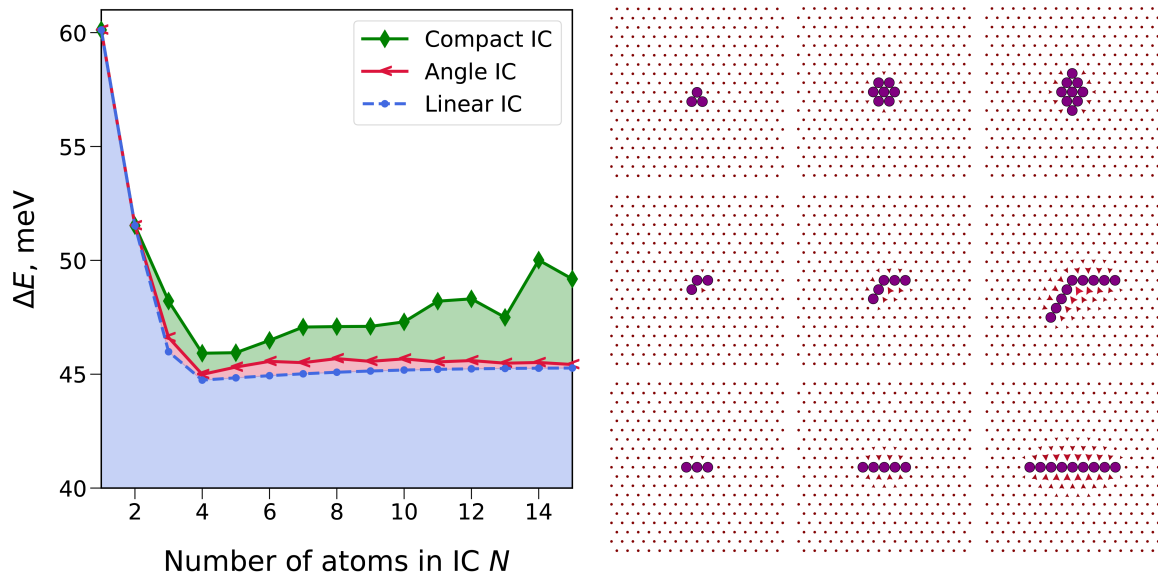


FIG. 1. (Left panel): Energy barrier for nucleation as a function of the number of atoms in the IC, shown for three types: compact, angled, and linear. (Right panel): Dark circles indicate IC atoms for compact (top row), angled (middle row), and linear (bottom row) configurations. Arrows represent the magnetization orientation in the ground state.

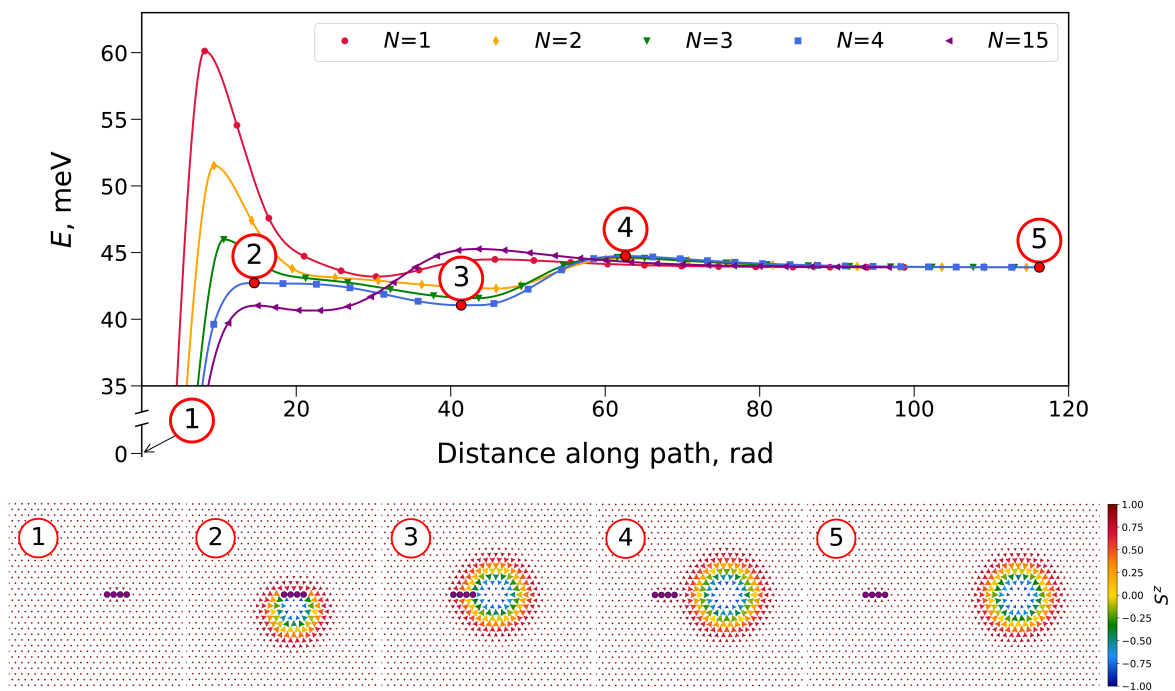


FIG. 2. MEPs for the nucleation of a Sk at linear IC of various sizes. The insets in the bottom show magnetic configurations along the MEP in case $N = 4$. States 1, 3 and 5 correspond to minima, state 2 corresponds to saddle point of creation and state 4 to saddle point of depinning from IC. The color in insets indicates the value of the out-of-plane component of the magnetic moments.

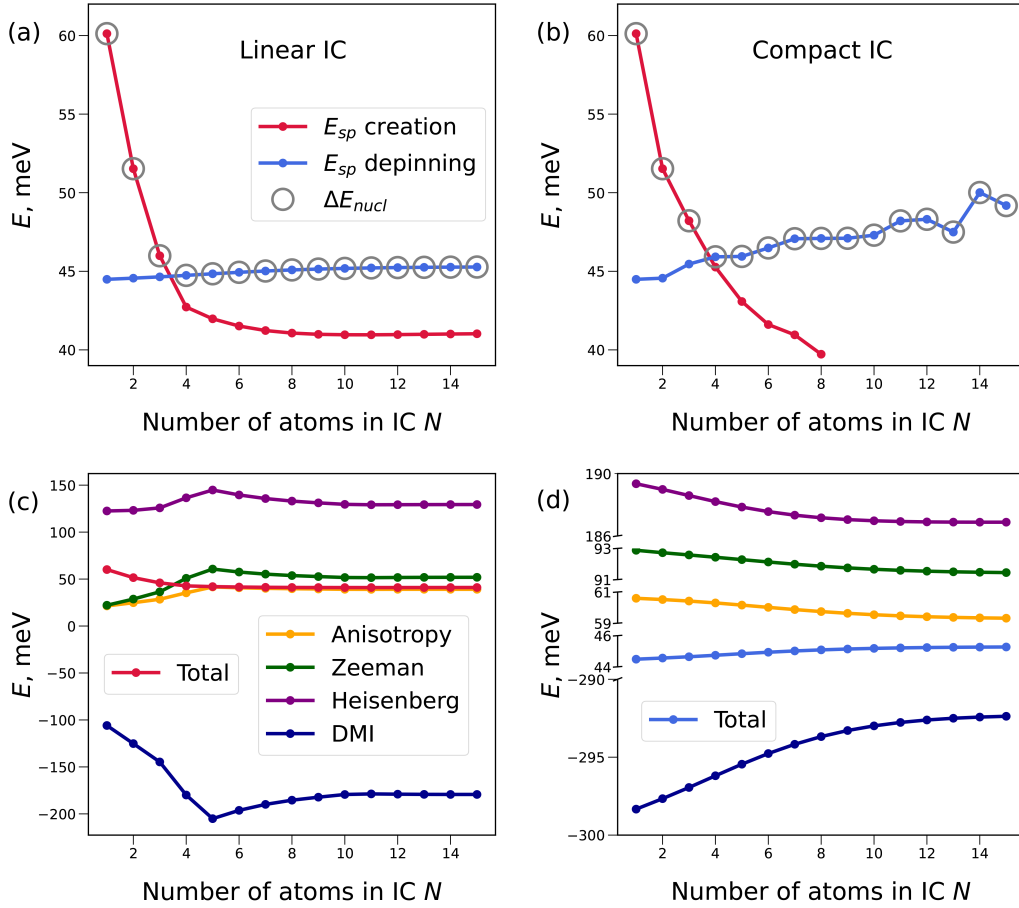


FIG. 3. Energy of saddle points for creation and depinning as a function of size of IC for line type (a) and for compact type (b). The dominant energy is indicated by empty circles. Energy contributions to saddle point for creation (c) and depinning (d) from linear IC as a function of N . Total energy in (c) corresponds to the energy of saddle point for creation, shown in red in (a). Total energy in (d) corresponds to the energy of saddle point for depinning, shown in blue in (a). Labels for Anisotropy, Zeeman, Heisenberg and DMI energy are the same for (c) and (d).

(indicated by empty circles in Fig. 3a). The maximum determines energy barrier in Fig. 1. We are interested in identifying the optimal value of N at which the nucleation barrier is minimized, thus Sk nucleation is fastest. Since both dependencies are monotonic, this minimum occurs at their intersection. In our case, with discrete values of N , the optimal size is the smallest N at which the barrier for depinning exceeds that for creation. Thus, in our analysis, we find that $N_{opt} = 4$.

To explain the contrasting behaviour of the barriers as N increases in Fig. 3a, we examine the spin configurations at the saddle points for both creation and depinning across three different sizes, along with the corresponding energy density distributions (see Figs. 4 and 5). During the creation process, we observe that the impurity is situated in a region of maximum positive energy (relatively the FM state). Introducing an IC – essentially removing atoms from this region – results in a decrease in energy. For small N , as illustrated in Figs. 4a and b, an increase in the size of the linear IC is accompanied by an increase in the radius of the saddle point. In this case, a larger radius of the Sk-like transition state configuration leads to a reduction in energy, since exchange energy in a micromagnetic framework behaves as R^{-1} for small R [36]. It is worth noting that the presence of the IC allows the Sk to bypass the small-radius phase during creation, since its minimum diameter is constrained by the size of the IC. Thus, two factors contribute to the sharp decrease in creation energy at small N : the increase in the subtracted positive energy as the IC size increases and the expansion of the saddle point radius.

At the saddle point, the energy densities associated with exchange, anisotropy, and Zeeman terms are positive, while the DMI energy density is negative. In the outer region of Sk, the DMI contribution dominates, resulting in a negative total energy density, whereas in the inner region, the other contributions prevail, leading to a positive total energy density. Introducing vacancies without changing the radius of the transition state would typically reduce the total energy, as the vacancies lie in the inner region of the Sk along the MEP. However, if the shape of the saddle point is assumed to remain fixed, the energy should decrease monotonically with the addition of impurities. This monotonic decrease is not observed

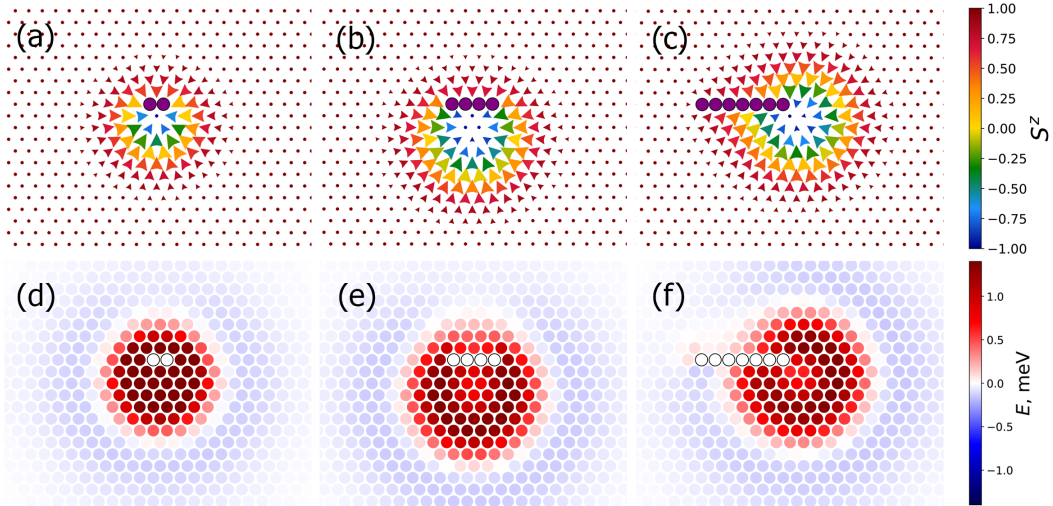


FIG. 4. Creation of Sk at linear IC: spin configurations of saddle point for $N=2, 4$ and 7 (a, b, c) and corresponding distribution of energy per atom (d, e, f).

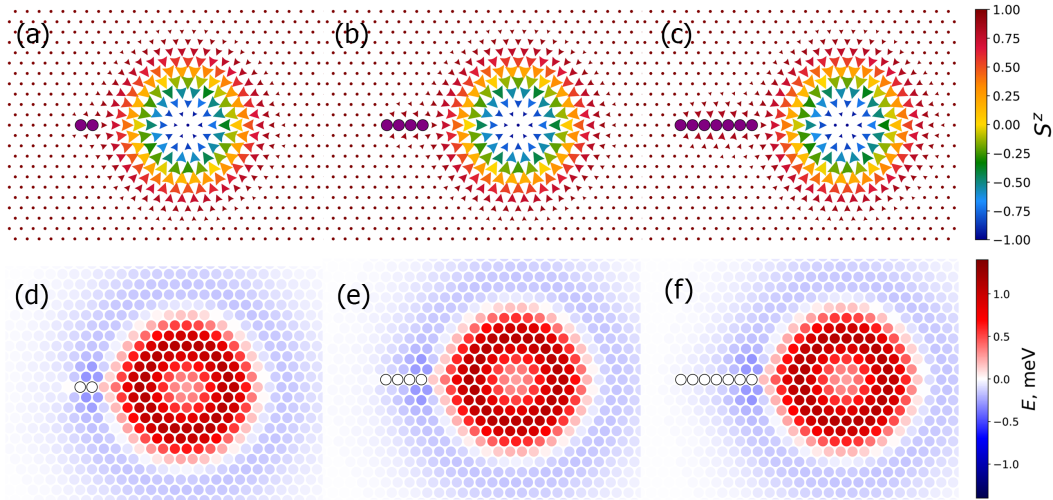


FIG. 5. Depinning of Sk from linear IC: spin configurations of saddle point for $N=2, 4$ and 7 (a, b, c) and corresponding distribution of energy per atom (d, e, f).

in Fig. 3c, which shows that the contributions from anisotropy, Zeeman, and symmetric exchange interactions actually increase at small N . This indicates that the energy reduction due to an increasing Sk radius has a stronger effect than the energy reduction from IC removal alone.

Inside the Sk, the energy density is positive, so removing atoms from this region reduces the energy barrier. However, it is energetically unfavourable for the saddle-point configuration to exceed the typical size of the Sk. As a result, beyond a certain IC size (in our case, $N = 5$), the IC can no longer be fully contained within the positive-energy region. At this point, some IC atoms extend into areas of zero or even negative energy density (see Fig. 4c), diminishing the effectiveness of energy reduction. This explains why the energy contributions in Fig. 3c exhibit a change of trend at point $N=5$. From the energy density distribution shown in Figs. 4d, e, and f, it is evident that in the negative energy regions, the energy density is relatively low and decreases gradually. This behaviour explains why the energy for creation begins to change only slightly for $N > 5$ (as depicted in Fig. 3a).

The depinning process involves the transition from a Sk localized at an IC to a free Sk. The saddle-point configurations associated with this process (see Fig. 5, upper panel) can be qualitatively understood as follows. The energy density distribution (Fig. 5, lower panel), shows that the maximum of positive energy in the inner region of the Sk decreases with radial distance r from the center, becomes negative, and reaches a minimum at a finite distance R_1 . Beyond $r > R_1$, the negative energy density decreases in magnitude with further increase in r . As the Sk detaches from the IC, it traverses this region of negative energy. Introducing an IC into this region effectively removes contributions with negative energy,

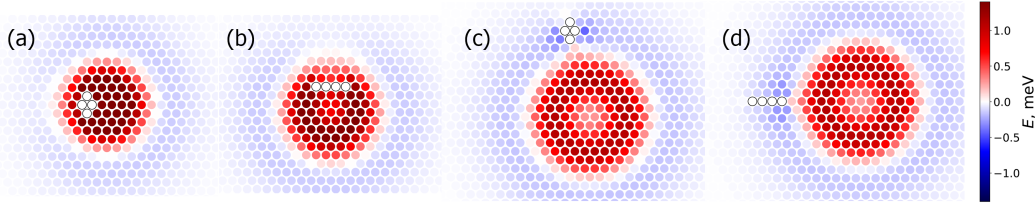


FIG. 6. Distribution of energy per atom in transition state for creation and depinning of Sk from compact IC (a) and (c) and linear IC (b) and (d).

thus increasing the total energy. Consequently, the maximum energy along the depinning path occurs when the IC coincides with the region of minimum energy density. Since we are interested in the minimum energy path, the path must be arranged to minimize this maximum energy. The total energy also depends on the orientation of the linear IC relative to the Sk's radial direction. Because the negative energy density diminishes for $r > R_1$, the lowest-energy configuration is achieved when the IC is aligned radially with respect to the Sk.

Adding atoms to the IC corresponds to removing additional atoms from the negative energy region, progressively further from the Sk center (see Fig. 5d, e, f). As shown, the energy density in the negative region is relatively low compared to that in the central part and also decreases with increasing distance from the center. This behavior accounts for the minimal change in the depinning barrier as N increases, as shown in Fig. 3a. It is worth noting that the variation in the depinning barrier with N is primarily driven by changes in the DMI energy contribution, as illustrated in Fig. 3d, which plots the energy components at the depinning saddle point as a function of N .

Effect of IC Geometry on Nucleation Barrier. In the previous section, we analyzed the influence of linear IC size on Sk nucleation. Another key factor is the geometry of the IC maximizing Sk nucleation rate. As mentioned earlier, for all values of N , linear ICs yield lower nucleation barriers compared to angular and compact ICs geometries. To understand the origin of this trend, we examine nucleation on compact IC more closely. During the Sk creation process, a compact IC – like a linear one – is located in a region of maximum energy. However, the radius of the saddle point associated with a compact IC is smaller (see Fig. 6a, b), leading to a higher creation barrier compared to that of a linear IC for N values up to 6 (as shown by the red curves in Fig. 3).

As previously noted, for $N > 6$, the linear IC no longer fits entirely within the Sk and begins to overlap with regions of negative energy, whereas the compact IC remains fully confined to the positive energy region. In this regime, the compact IC exhibits a lower creation barrier than the linear one (see $N = 7$ and 8 in Fig. 3a and b).

Regarding the depinning process, a linear IC consistently yields a lower energy barrier than a compact IC for all values of N (see Fig. 3a and b). This can be attributed to the fact that a compact IC, situated in the region of minimum negative energy, will inevitably remove atoms with a higher magnitude of negative energy (Fig. 6c), whereas a linear IC extends along the gradient where the negative energy density gradually decreases (Fig. 6d).

The crossover point between the creation and depinning barriers for a compact IC occurs at $N = 4$. For smaller N , the creation barrier dominates and is higher for compact ICs than for linear ones. For $N \geq 4$, the depinning barrier becomes dominant and remains higher for compact ICs as well. As a result, the nucleation barrier for a compact IC exceeds that for a linear IC across all values of N , as shown in Fig. 1.

It is worth noting that the depinning energy varies non-monotonically with N for compact ICs (Fig. 3b). This nonmonotonic behavior arises because adding impurities can create sharp angles that contribute to a reduction in the depinning barrier.

It is also important to note that the creation process for compact ICs effectively “disappears” when the size reaches $N = 9$ (see Fig. 3b). As demonstrated in the work by Potkina et al. [7], as the size of the compact IC increases, the barrier for the collapse of the Sk localized on it decreases, ultimately reaching zero at $N = 9$. Consequently, the metastable state associated with the Sk localized on the IC vanishes, leading to a transition from a two-stage nucleation process to a single process in which a Sk is created while simultaneously detaching from the IC.

In addition to the types of ICs discussed, intermediate variants are also possible, such as an angular IC. This type differs from a linear IC by having a break at one point, resulting in a more compact shape, which leads to intermediate values of nucleation energies, as shown in Fig. 1. As can be observed, the difference between the energies associated with an angular IC and those of a linear IC is not high. Therefore, minor imperfections in the fabrication of a linear IC do not significantly compromise the effect of reducing the nucleation energy.

4. Discussion

Based on the calculated energies of the transition states, we have identified a trend indicating that elongated ICs are more favorable for Sk nucleation compared to compact ones. We have provided a qualitative explanation for this observed effect, independent of the specific parameters of Hamiltonian (1) and the type of lattice used. This supports the universality of our findings.

In addition to geometry, the size of the linear IC also influences the nucleation energy. An increase in the IC size reduces the barrier for creation, but simultaneously raises the barrier for depinning. Therefore, the optimal size is determined by balancing the energies of the transition states for creation and depinning. Since these energies generally depend on the parameters of the system, the optimal IC size will also vary accordingly. It is important to note that for certain system parameters, there may be no crossover between the energies of creation and depinning, or nucleation may occur in a single stage without an intermediate minimum corresponding to a Sk localized on the IC. These scenarios warrant further investigation.

The superiority of the linear defect geometry is further supported by our earlier findings on nucleation at boundary defects [37]. We discovered that among all possible notch geometries, the most favorable configuration for nucleation is a needle-shaped notch with sufficient depth. However, this option is still less effective than a linear IC. For instance, in the studied PdFe/Ir(111) system at a magnetic field of $B = 3.75$ T, the nucleation barrier for a needle-shaped notch is 45.65 meV, whereas for a linear IC consisting of 4 atoms, it is 44.74 meV, resulting in an energy gain of approximately 2%. This difference arises from the additional exclusion of atoms from the region of negative energy density in the case of the notch, which adversely affects the energy required for depinning.

It is interesting to compare nucleation on ICs with other types of Sk nucleation on a track that we have previously investigated [6]. The barriers for Sk nucleation within the track and at its boundary were found to be 85.07 meV and 75.62 meV, respectively. In contrast, a linear IC of optimal size, as well as a needle-shaped notch, can reduce the nucleation barriers by nearly half in the PdFe/Ir(111) system under consideration at a magnetic field of $B = 3.75$ T.

The energies of the saddle points for creation and depinning are measured from a homogeneous FM state with an IC that does not contain a Sk. To investigate the reverse process – the annihilation of a Sk on ICs – the obtained energies of the transition states should be referenced from the energy of a free Sk, which is independent of the shape and geometry of the IC. Consequently, the behavior of the transition state energies for pinning and collapse qualitatively aligns with those reported for creation and depinning. This indicates that, for erasing information, it is also most advantageous to utilize a linear IC of optimal size.

In experimental studies [38–41], notches at boundaries have been employed to create Sk. Our findings suggest that boundary notches of any geometry are less energy-efficient for Sk creation compared to a linear defect. It is also worth noting that the minimum possible nucleation barrier is determined by the difference in the energy of the final free Sk and the energy of the initial ferromagnetic state. A linear cluster of optimal size yields a barrier only slightly higher than this value (44.74 meV versus 43.9 meV). We hope that these results will encourage further experimental research into Sk nucleation at defects.

In summary, we have demonstrated that a linear defect of optimal size minimizes the energy required for Sk nucleation, which could be advantageous in the design of Sk-based magnetic memory and computing devices.

References

- [1] Bogdanov A.N., Rössler U.K. Chiral Symmetry Breaking in Magnetic Thin Films and Multilayers. *Phys. Rev. Lett.*, 2001, **87**, P. 037203.
- [2] Romming N., Hanneken C., Menzel M., Bickel J.E., Wolter B., von Bergmann K., Kubetzka A., Wiesendanger R. Writing and Deleting Single Magnetic Skyrmions. *Science*, 2013, **341**(6146), P. 636–639.
- [3] Fert A., Cros V., Sampaio J. Skyrmions on the track. *Nat. Nanotechnol.*, 2013, **8**, P. 152–156.
- [4] Woo S., Litzius K., Krüger B., Im M.-Y., Caretta L., Richter K., Mann M., Krone A., Reeve R. M., Weigand M., Agrawal P., Lemesh I., Mawass M.-A., Fischer P., Kläui M., Beach G. S. D. Observation of room-temperature magnetic skyrmions and their current-driven dynamics in ultrathin metallic ferromagnets. *Nat. Mater.*, 2016, **15**, P. 501.
- [5] Uzdin V.M., Potkina M.N., Lobanov I.S., Bessarab P.F., Jónsson H. The effect of confinement and defects on the thermal stability of skyrmions. *Physica B: Condensed Matter*, 2018, **549**, P. 6–9.
- [6] Uzdin V.M., Potkina M.N., Lobanov I.S., Bessarab P.F., Jónsson H. Energy surface and lifetime of magnetic skyrmions. *J. Magn. Magn. Mater.*, 2018, **459**, P. 236–240.
- [7] Potkina M.N., Lobanov I.S., Uzdin V.M. Nonmagnetic impurities in skyrmion racetrack memory. *Nanosystems: Phys., Chem., Math.*, 2020, **11**(6), P. 628–635.
- [8] Stosic D., Luderer B.T., Milošević V.M. Pinning of magnetic skyrmions in a monolayer Co film on Pt(111): Theoretical characterization and exemplified utilization. *Phys. Rev. B*, 2017, **96**(21), P. 214403.
- [9] Fernandes I.L., Bouaziz J., Blügel S., Lounis S. Universality of defect-skyrmion interaction profiles. *Nat. Commun.*, 2018, **9**(1), P. 4395.
- [10] Castell-Queralt J., González-Gómez L., Del-Valle N., Sanchez A., Navau C. Accelerating, guiding, and compressing skyrmions by defect rails. *Nanoscale*, 2019, **11**(26), P. 12589–12594.
- [11] Suess D., Vogler C., Bruckner F., Heistracher P., Slanovc F., Abert C. Spin torque efficiency and analytic error rate estimates of skyrmion. *Sci. Rep.*, 2019, **9**, P. 4827.
- [12] Morshed M.G., Vakili H., Ghosh A.W. Positional stability of skyrmions in a racetrack memory with notched geometry. *Phys. Rev. Applied*, 2022, **17**, P. 064019.
- [13] Belrhazi H., El Hafidi M. Nucleation and manipulation of single skyrmions using spin-polarized currents in antiferromagnetic skyrmion-based racetrack memories. *Sci. Rep.*, 2022, **12**, P. 15225.
- [14] Hanneken C., Kubetzka A., von Bergmann K., Wiesendanger R. Pinning and movement of individual nanoscale magnetic skyrmions via defects. *New J. Phys.*, 2016, **18**(5), P. 055009.
- [15] Li W., Wang X., Dai Y., Bian Y., Huang Q., Zhang X., Su L., Zhang B., Tang D., Yang Y. Voltage-controlled skyrmion deletion device based on magnetic defects. *J. Phys. D: Appl. Phys.*, 2021, **54**, P. 445001.
- [16] Potkina M.N., Lobanov I.S., Uzdin V.M. Fine energy structure of a magnetic skyrmion localized on a nonmagnetic impurity in an external magnetic field. *Physics of Complex Systems*, 2020, **1**(4), P. 165–168.

- [17] Choi H.C., Lin S.Z., Zhu J.X. Density functional theory study of skyrmion pinning by atomic defects in MnSi. *Phys. Rev. B*, 2016, **93**, P. 115112.
- [18] Arjana I.G., Fernandes I.L., Chico J., Lounis S. Sub-nanoscale atom-by-atom crafting of skyrmion-defect interaction profiles. *Sci. Rep.*, 2020, **10**, P. 14655.
- [19] Iwasaki J., Mochizuki M., Nagaosa N. Universal current-velocity relation of skyrmion motion in chiral magnets. *Nat. Commun.*, 2013, **4**(1), P. 1463.
- [20] Koshibae W., Nagaosa N. Theory of current-driven skyrmions in disordered magnets. *Sci. Rep.*, 2018, **8**(1), P. 6328.
- [21] Toscano D., Leonel S.A., Coura P.Z., Sato F. Building traps for skyrmions by the incorporation of magnetic defects into nanomagnets: Pinning and scattering traps by magnetic properties engineering. *J. Magn. Magn. Mater.*, 2019, **480**, P. 171.
- [22] Everschor-Sitte K., Sitte M., Valet T., Abanov A., Sinova J. Skyrmion production on demand by homogeneous DC currents. *New J. Phys.*, 2017, **19**, P. 092001.
- [23] Mulkers J., Waeyenberge B.V., Milošević M.V. Effects of spatially engineered Dzyaloshinskii-Moriya interaction in ferromagnetic films. *Phys. Rev. B*, 2017, **95**, P. 144401.
- [24] Derras-Chouk A., Chudnovsky E.M. Skyrmions near defects. *J. Phys.: Condens. Matter*, 2021, **33**, P. 195802.
- [25] Müller J., Rosch A. Capturing of a magnetic skyrmion with a hole. *Phys. Rev. B*, 2015, **91**(5), P. 054410.
- [26] Liu Y.H., Li Y.Q. A mechanism to pin skyrmions in chiral magnets. *J. Phys.: Condens. Matter*, 2013, **25**, P. 076005.
- [27] Martínez J.C., Jalil M.B.A. Topological dynamics and current-induced motion in a skyrmion lattice. *New J. Phys.*, 2016, **18**, P. 033008.
- [28] Navau C., Del-Valle N., Sanchez A. Interaction of isolated skyrmions with point and linear defects. *J. Magn. Magn. Mater.*, 2018, **465**, P. 709.
- [29] Lin S.Z., Reichhardt C., Batista C.D., Saxena A. Particle model for skyrmions in metallic chiral magnets: Dynamics, pinning, and creep. *Phys. Rev. B*, 2013, **87**, P. 214419.
- [30] González-Gómez L., Castell-Queralt J., Del-Valle N., Sanchez A., Navau C. Analytical modeling of the interaction between skyrmions and extended defects. *Phys. Rev. B*, 2019, **100**, P. 054440.
- [31] Hagemeister J., Romming N., von Bergmann K., Vedmedenko E.Y., Wiesendanger R. Stability of single skyrmionic bits. *Nat. Commun.*, 2015, **6**(1), P. 8455.
- [32] Lobanov I.S., Uzdin V.M. The lifetime of micron scale topological chiral magnetic states with atomic resolution. *Comp. Phys. Commun.*, 2021, **269**, P. 108136.
- [33] Bessarab P.F., Uzdin V.M., Jónsson H. Harmonic transition-state theory of thermal spin transitions. *Phys. Rev. B*, 2012, **85**(18), P. 184409.
- [34] Weinan E., Ren W., Vanden-Eijnden E. String method for the study of rare events. *Phys. Rev. B*, 2002, **66**, P. 052301.
- [35] Lobanov I.S., Potkina M.N., Jónsson H., Uzdin V.M. Truncated minimum energy path method for finding first order saddle points. *Nanosystems: Phys., Chem., Math.*, 2017, **8**(5), P. 586–595.
- [36] Wang X.S., Yuan H.Y., Wang X.R. A theory on skyrmion size. *Commun. Phys.*, 2018, **1**, P. 31.
- [37] Potkina M.N., Lobanov I.S. Nucleation of magnetic skyrmions at a notch. *Nanosystems: Phys., Chem., Math.*, 2024, **15**(2), P. 192–200.
- [38] Wang W., Song D., Wei W., Nan P., Zhang S., Ge B., Tian M., Zang J., Du H. Electrical manipulation of skyrmions in a chiral magnet. *Nat. Commun.*, 2022, **13**, P. 1593.
- [39] Yu X. Z., Morikawa D., Nakajima K., Shibata K., Kanazawa N., Arima T., Nagaosa N., Tokura Y. Motion tracking of 80-nm-size skyrmions upon directional current injections. *Sci. Adv.*, 2020, **6**, P. eaaz9744.
- [40] Twitchett-Harrison A.C., Loudon J.C., Pepper R.A., Birch M.T., Fangohr H., Midgley P.A., Balakrishnan G., Hatton P.D. Confinement of skyrmions in nanoscale FeGe device-like structures. *ACS Appl. Electron. Mater.*, 2022, **4**(9), P. 4427–4437.
- [41] Büttner F., Lemesh I., Schneider M., Pfau B., Günther C.M., Hessian P., Geilhufe J., Caretta L., Engel D., Krüger B., Viehhaus J., Eisebitt S., Beach G.S.D. Field-free deterministic ultrafast creation of magnetic skyrmions by spin-orbit torques. *Nat. Nanotech.*, 2017, **12**, P. 1040–1044.

Submitted 12 April 2025; revised 29 May 2025; accepted 30 May 2025

Information about the authors:

Maria N. Potkina – Infochemistry Scientific Center, ITMO University, 197101 St. Petersburg, Russia; ORCID 0000-0002-1380-2454; potkina.maria@yandex.ru

Igor S. Lobanov – Faculty of Physics, ITMO University, 197101 St. Petersburg, Russia; ORCID 0000-0001-8789-3267; lobanov.igor@gmail.com

Conflict of interest: the authors declare no conflict of interest.